J|A|C|S
ARTICLES
Published on Web 04/03/2002

Theoretical Investigation of Large Kinetic Isotope Effects for Proton-Coupled Electron Transfer in Ruthenium Polypyridyl Complexes

Nedialka Iordanova and Sharon Hammes-Schiffer*

Contribution from the Department of Chemistry, 152 Davey Laboratory, The Pennsylvania State University, University Park, Pennsylvania 16802

Received November 28, 2001

Abstract: A theoretical investigation of proton-coupled electron transfer in ruthenium polypyridyl complexes is presented. The three reactions studied are as follows: (1) the comproportionation reaction of $[(bpy)_2(py)Ru^{IV}O]^{2+}$ and $[(bpy)_2(py)Ru^{II}OH_2]^{2+}$ to produce $[(bpy)_2(py)Ru^{III}OH]^{2+}$; (2) the comproportionation reaction of $[(tpy)(bpy)Ru^{IV}O]^{2+}$ and $[(tpy)(bpy)Ru^{II}OH_2]^{2+}$ to produce $[(tpy)(bpy)Ru^{III}OH]^{2+}$; and (3) the cross reaction of $[(tpy)(bpy)Ru^{III}OH]^{2+}$ and $[(bpy)_2(py)Ru^{II}OH_2]^{2+}$ to produce $[(tpy)(bpy)Ru^{II}OH_2]^{2+}$ and $[(bpy)_2(py)Ru^{III}OH]^{2+}$. This investigation is motivated by experimental measurements of rates and kinetic isotope effects for these systems (Binstead, R. A.; Meyer, T. J. *J. Am. Chem. Soc.* **1987**, *109*, 3287. Farrer, B. T.; Thorp, H. H. *Inorg. Chem.* **1999**, *38*, 2497.). These experiments indicate that the second reaction is nearly one order of magnitude faster than the first reaction, and the third reaction is in the intermediate regime. The experimentally measured kinetic isotope effects for these three reactions are 16.1, 11.4, and 5.8, respectively. The theoretical calculations elucidate the physical basis for the experimentally observed trends in rates and kinetic isotope effects, as well as for the unusually high magnitude of the kinetic isotope effects. In this empirical model, the proton donor−acceptor distance is predicted to be largest for the first reaction and smallest for the third reaction. This prediction is consistent with the degree of steric crowding near the oxygen proton acceptor for the three reactions. The second reaction is faster than the first reaction since a smaller proton donor−acceptor distance leads to a larger overlap between the reactant and product proton vibrational wave functions. The intermediate rate of the third reaction is determined by a balance among several competing factors. The observed trend in the kinetic isotope effects arises from the higher ratio of the hydrogen to deuterium vibrational wave function overlap for larger proton donor−acceptor distances. Thus, the kinetic isotope effect increases for larger proton donor-acceptor distances. The unusually high magnitude of the kinetic isotope effects is due in part to the close proximity of the proton transfer interface to the electron donor and acceptor. This proximity results in strong electrostatic interactions that lead to a relatively small overlap between the reactant and product vibrational wave functions.

I. Introduction

The coupling between proton and electron transfer reactions is crucial for a wide range of chemical and biological processes. As a result, the illumination of the fundamental principles of proton-coupled electron transfer (PCET) reactions is of great interest.[1−6] Experimental studies have provided rates and kinetic isotope effects for numerous model PCET reactions in solution.[7−13] (Here the kinetic isotope effect refers to the ratio of the rate with hydrogen to the rate with deuterium.) Although the majority of the kinetic isotope effects are moderate (i.e., between one and three),[10,13] unusually high kinetic isotope effects of up to 16 have been observed at room temperature for PCET reactions in ruthenium polypyridyl complexes.[7−9] These large kinetic isotope effects imply the importance of nuclear quantum effects such as hydrogen tunneling. The theoretical investigation of reactions with high kinetic isotope effects provides a unique opportunity to clarify the role of such nuclear quantum effects in PCET reactions. This clarification will aid in the elucidation of the basic mechanism for the coupling of electron and proton transfer reactions.

* To whom correspondence should be addressed. E-mail: shs@chem.psu.edu.

(1) Cukier, R. I. *J. Phys. Chem.* **1994**, *98*, 2377. Cukier, R. I. *J. Phys. Chem.* **1996**, *100*, 15428.
(2) Cukier, R. I.; Nocera, D. G. *Annu. Rev. Phys. Chem.* **1998**, *49*, 337.
(3) Hammes-Schiffer, S. *Acc. Chem. Res.* **2001**, *34*, 273.
(4) Hammes-Schiffer, S. In *Electron Transfer in Chemistry Vol. I: Principles, Theories, Methods, and Techniques*; Balzani, V., Ed.; Wiley-VCH: Weinheim, 2001.
(5) Georgievskii, Y.; Stuchebrukhov, A. A. *J. Chem. Phys.* **2000**, *113*, 10438.
(6) Roth, J. P.; Yoder, J. C.; Won, T. J.; Mayer, J. M. *Science* **2001**, *294*, 2524.
(7) Binstead, R. A.; Moyer, B. A.; Samuels, G. J.; Meyer, T. J. *J. Am. Chem. Soc.* **1981**, *103*, 2897.
(8) Binstead, R. A.; Meyer, T. J. *J. Am. Chem. Soc.* **1987**, *109*, 3287.
(9) Farrer, B. T.; Thorp, H. H. *Inorg. Chem.* **1999**, *38*, 2497.
(10) Weatherly, S. C.; Yang, I. V.; Thorp, H. H. *J. Am. Chem. Soc.* **2001**, *123*, 1236.
(11) Turro, C.; Chang, C. K.; Leroi, G. E.; Cukier, R. I.; Nocera, D. G. *J. Am. Chem. Soc.* **1992**, *114*, 4013.
(12) Kirby, J. P.; Roberts, J. A.; Nocera, D. G. *J. Am. Chem. Soc.* **1997**, *119*, 9230.
(13) Roth, J. P.; Lovel, S.; Mayer, J. M. *J. Am. Chem. Soc.* **2000**, *122*, 5486.

10.1021/ja017633d CCC: $22.00

We have developed a theoretical formulation for PCET that includes both electronic and nuclear quantum effects.[3,4,14−16] Recently we performed a comparative theoretical investigation of single electron transfer (ET), single proton transfer (PT), and PCET reactions in iron bi-imidazoline complexes.[17] These calculations were motivated by experimental studies of Mayer and co-workers indicating that the rates of ET and PCET are similar and that the kinetic isotope effect for PCET is 2.3.[13] The theory accurately reproduced the experimentally measured rates and kinetic isotope effects for ET and PCET. The calculations showed that the similarity of the rates for ET and PCET is due mainly to the compensation of the larger outer-sphere solvent reorganization energy for ET by the smaller coupling for PCET caused by averaging over the reactant and product vibrational wave functions. The moderate kinetic isotope effect for PCET was found to arise from the relatively large overlap between the reactant and product vibrational wave functions. The application of this theory to photoinduced PCET through amidinium−carboxylate salt bridges also resulted in moderate kinetic isotope effects.[18,19]

In this paper, we apply our theoretical formulation for PCET to reactions with high kinetic isotope effects. Specifically, we focus on the following reactions:

$$[(bpy)_2(py)Ru^{II}OH_2]^{2+} + [(bpy)_2(py)Ru^{IV}O]^{2+} \rightleftharpoons [(bpy)_2(py)Ru^{III}OH]^{2+} + [(bpy)_2(py)Ru^{III}OH]^{2+} \quad (1)$$

$$[(tpy)(bpy)Ru^{II}OH_2]^{2+} + [(tpy)(bpy)Ru^{IV}O]^{2+} \rightleftharpoons [(tpy)(bpy)Ru^{III}OH]^{2+} + [(tpy)(bpy)Ru^{III}OH]^{2+} \quad (2)$$

$$[(bpy)_2(py)Ru^{II}OH_2]^{2+} + [(tpy)(bpy)Ru^{III}OH]^{2+} \rightleftharpoons [(bpy)_2(py)Ru^{III}OH]^{2+} + [(tpy)(bpy)Ru^{II}OH_2]^{2+} \quad (3)$$

(Here tpy = 2,2′:6′,2″-terpyridine, bpy = 2,2′-bipyridine, and py = pyridine.) The two comproportionation reactions are denoted CompA (eq 1) and CompB (eq 2), and the cross reaction is denoted Cross (eq 3). These three reactions are depicted in Figure 1. The CompA and Cross reactions were studied experimentally by Meyer and co-workers,[7,8] and the CompB reaction was studied experimentally by Farrer and Thorp.[9] Thus, the experimentally determined rates and kinetic isotope effects, as well as the driving forces, are available for all of these reactions. Correcting for differences in ionic strength, the CompB reaction is nearly one order of magnitude faster than the CompA reaction, and the Cross reaction is in the intermediate regime. Moreover, the kinetic isotope effects for the CompA, CompB, and Cross reactions are 16.1, 11.4, and 5.8, respectively. Our theoretical investigation of these reactions elucidates the physical basis for the experimentally observed trends in rates and kinetic isotope effects, as well as for the unusually high magnitude of the kinetic isotope effects.

II. Theory and Methods

Fundamental Theory. The theoretical formulation for PCET utilized in this paper is based on the recently developed

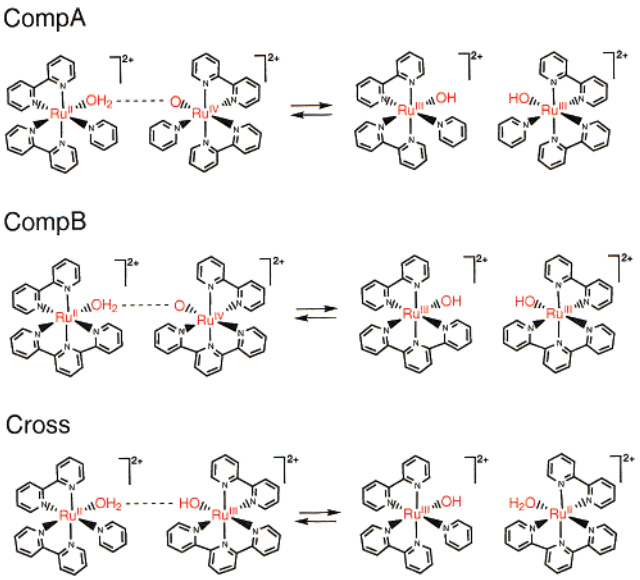

Figure 1. The three ruthenium polypyridyl reactions studied in this paper.

multistate continuum theory.[4,14,15] In this theory, a PCET reaction is represented by four diabatic states that are defined within a valence bond approach. The four diabatic states are labeled 1a, 1b, 2a, and 2b, where the label 1 or 2 indicates the ET state and the label a or b indicates the PT state. For the CompA reaction, the diabatic states are

$$\text{(1a)}\quad [(bpy)_2(py)Ru^{II}OH_2]^{2+} + [(bpy)_2(py)Ru^{IV}O]^{2+}$$

$$\text{(1b)}\quad [(bpy)_2(py)Ru^{II}OH]^{+} + [(bpy)_2(py)Ru^{IV}OH]^{3+}$$

$$\text{(2a)}\quad [(bpy)_2(py)Ru^{III}OH_2]^{3+} + [(bpy)_2(py)Ru^{III}O]^{+}$$

$$\text{(2b)}\quad [(bpy)_2(py)Ru^{III}OH]^{2+} + [(bpy)_2(py)Ru^{III}OH]^{2+} \quad (4)$$

For the CompB reaction, the diabatic states are

$$\text{(1a)}\quad [(tpy)(bpy)Ru^{II}OH_2]^{2+} + [(tpy)(bpy)Ru^{IV}O]^{2+}$$

$$\text{(1b)}\quad [(tpy)(bpy)Ru^{II}OH]^{+} + [(tpy)(bpy)Ru^{IV}OH]^{3+}$$

$$\text{(2a)}\quad [(tpy)(bpy)Ru^{III}OH_2]^{3+} + [(tpy)(bpy)Ru^{III}O]^{+}$$

$$\text{(2b)}\quad [(tpy)(bpy)Ru^{III}OH]^{2+} + [(tpy)(bpy)Ru^{III}OH]^{2+} \quad (5)$$

For the Cross reaction, the diabatic states are

$$\text{(1a)}\quad [(bpy)_2(py)Ru^{II}OH_2]^{2+} + [(tpy)(bpy)Ru^{III}OH]^{2+}$$

$$\text{(1b)}\quad [(bpy)_2(py)Ru^{II}OH]^{+} + [(tpy)(bpy)Ru^{III}OH_2]^{3+}$$

$$\text{(2a)}\quad [(bpy)_2(py)Ru^{III}OH_2]^{3+} + [(tpy)(bpy)Ru^{II}OH]^{+}$$

$$\text{(2b)}\quad [(bpy)_2(py)Ru^{III}OH]^{2+} + [(tpy)(bpy)Ru^{II}OH_2]^{2+} \quad (6)$$

As shown in ref 14, the free energy surfaces for PCET reactions may be calculated as functions of two collective solvent coordinates z_p and z_e, corresponding to PT and ET, respectively. The ET diabatic free energy surfaces corresponding to ET states 1 and 2 are calculated as mixtures of the a and b

(14) Soudackov, A. V.; Hammes-Schiffer, S. *J. Chem. Phys.* **1999**, *111*, 4672.
(15) Soudackov, A. V.; Hammes-Schiffer, S. *J. Chem. Phys.* **2000**, *113*, 2385.
(16) Decornez, H.; Hammes-Schiffer, S. *J. Phys. Chem. A* **2000**, *104*, 9370.
(17) Iordanova, N.; Decornez, H.; Hammes-Schiffer, S. *J. Am. Chem. Soc.* **2001**, *123*, 3723.
(18) Soudackov, A. V.; Hammes-Schiffer, S. *J. Am. Chem. Soc.* **1999**, *121*, 10598.
(19) Rostov, I.; Hammes-Schiffer, S. *J. Chem. Phys.* **2001**, *115*, 285.

PT states. The reactants (I) are mixtures of the 1a and 1b diabatic states, and the products (II) are mixtures of the 2a and 2b diabatic states. The proton vibrational states are calculated for both the reactant (I) and product (II) ET diabatic surfaces, resulting in two sets of two-dimensional free energy surfaces that may be approximated as paraboloids. In this theoretical formulation, the PCET reaction is described in terms of nonadiabatic transitions from the reactant (I) to the product (II) ET diabatic surfaces. (Here the ET diabatic states I and II, respectively, may be viewed as the reactant and product PCET states.)

The unimolecular rate expression derived in ref 15 for PCET is

$$k_{\mathrm{uni}}^{\mathrm{PCET}} = \frac{2\pi}{\hbar}\sum_{\mu} P_{\mathrm{I}\mu}\sum_{\nu} V_{\mu\nu}^2 (4\pi\lambda_{\mu\nu}k_{\mathrm{B}}T)^{-1/2} \exp\left\{\frac{-\Delta G_{\mu\nu}^{\dagger}}{k_{\mathrm{B}}T}\right\} \quad (7)$$

where $\sum_{\mu}$ and $\sum_{\nu}$ indicate a sum over vibrational states associated with ET states 1 and 2, respectively, $P_{\mathrm{I}\mu}$ is the Boltzmann factor for state Iμ, and

$$\Delta G_{\mu\nu}^{\dagger} = \frac{(\Delta G_{\mu\nu}^{\mathrm{o}} + \lambda_{\mu\nu})^2}{4\lambda_{\mu\nu}} \quad (8)$$

In this expression the free energy difference is defined as

$$\Delta G_{\mu\nu}^{\mathrm{o}} = \epsilon_{\nu}^{\mathrm{II}}(\bar{z}_{\mathrm{p}}^{\mathrm{II}\nu}, \bar{z}_{\mathrm{e}}^{\mathrm{II}\nu}) - \epsilon_{\mu}^{\mathrm{I}}(\bar{z}_{\mathrm{p}}^{\mathrm{I}\mu}, \bar{z}_{\mathrm{e}}^{\mathrm{I}\mu}) \quad (9)$$

where $(\bar{z}_{\mathrm{p}}^{\mathrm{I}\mu}, \bar{z}_{\mathrm{e}}^{\mathrm{I}\mu})$ and $(\bar{z}_{\mathrm{p}}^{\mathrm{II}\nu}, \bar{z}_{\mathrm{e}}^{\mathrm{II}\nu})$ are the solvent coordinates for the minima of the ET diabatic free energy surfaces $\epsilon_{\mu}^{\mathrm{I}}(z_{\mathrm{p}}, z_{\mathrm{e}})$ and $\epsilon_{\nu}^{\mathrm{II}}(z_{\mathrm{p}}, z_{\mathrm{e}})$, respectively. Moreover, the outer-sphere (solvent) reorganization energy is

$$\lambda_{\mu\nu} = \epsilon_{\mu}^{\mathrm{I}}(\bar{z}_{\mathrm{p}}^{\mathrm{II}\nu}, \bar{z}_{\mathrm{e}}^{\mathrm{II}\nu}) - \epsilon_{\mu}^{\mathrm{I}}(\bar{z}_{\mathrm{p}}^{\mathrm{I}\mu}, \bar{z}_{\mathrm{e}}^{\mathrm{I}\mu}) = \epsilon_{\nu}^{\mathrm{II}}(\bar{z}_{\mathrm{p}}^{\mathrm{I}\mu}, \bar{z}_{\mathrm{e}}^{\mathrm{I}\mu}) - \epsilon_{\nu}^{\mathrm{II}}(\bar{z}_{\mathrm{p}}^{\mathrm{II}\nu}, \bar{z}_{\mathrm{e}}^{\mathrm{II}\nu}) \quad (10)$$

The coupling $V_{\mu\nu}$ in the PCET rate expression given in eq 7 is defined as

$$V_{\mu\nu} = \langle \phi_{\mu}^{\mathrm{I}} | V(r_{\mathrm{p}}, z_{\mathrm{p}}^{\dagger}) | \phi_{\nu}^{\mathrm{II}} \rangle_{p} \quad (11)$$

where the subscript of the angular brackets indicates integration over r_{p}, $z_{\mathrm{p}}^{\dagger}$ is the value of z_{p} in the intersection region, and ϕ_{μ}^{I} and ϕ_{ν}^{II} are the proton vibrational wave functions for the reactant and product ET diabatic states, respectively. For the systems studied in this paper,

$$V_{\mu\nu} \approx V^{\mathrm{ET}} \langle \phi_{\mu}^{\mathrm{I}} | \phi_{\nu}^{\mathrm{II}} \rangle_{p} \quad (12)$$

where V^{ET} is the electronic coupling between states 1a and 2a and between states 1b and 2b. The physical basis for this approximation is discussed in ref 17, and its validity has been verified numerically for the three reactions studied in this paper.

The theoretical formulation described above is based on the assumption that the PCET reaction is nonadiabatic. An ET or PCET reaction is nonadiabatic if the coupling between the electron transfer states is much less than the thermal energy. A wide range of electronic couplings has been determined for ruthenium systems.[20,21] On the basis of the electronic characteristics and the distances involved, we expect ET and PCET to be electronically nonadiabatic for the systems studied in this paper. In addition, since the overlap between the dominant reactant and product proton vibrational wavefunctions is small, the overall coupling $V_{\mu\nu}$ for PCET is much less than the thermal energy.

Although the effects of inner-sphere solute modes are easily included in this theoretical formulation,[15,17] we neglect inner-sphere reorganization for the calculations presented in this paper. The frequencies of $Ru^{IV}-O$ bonds have been measured,[22,23] but to our knowledge the frequencies for the $Ru^{III}-OH$ and $R^{II}-OH_2$ bonds are not known. Thus, we are unable to calculate the inner-sphere reorganization energies for these systems. The inner-sphere reorganization energy is expected to be substantial for these systems due to the relatively high frequency ($\sim$800 cm^{-1}) of the $Ru^{IV}-O$ bonds and the significant change in the Ru−O distances. On the other hand, we do not expect the inner-sphere reorganization energy to significantly alter the trends in the relative rates and kinetic isotope effects. To test the impact of neglecting the inner-sphere reorganization energy, we recalculated the rates including an inner-sphere reorganization energy of 8 kcal/mol for all three reactions. Although the quantitative values changed, the trends in the relative rates and kinetic isotope effects were not altered. Hence, the neglect of the inner-sphere reorganization energy is not expected to influence the general conclusions of this paper. (Note that the inner-sphere reorganization energy of the Cross reaction is expected to differ from the inner-sphere reorganization energies of the CompA and CompB reactions, and this difference could impact the relative rate of the Cross reaction.)

Calculating Input Quantities. Within the framework of multistate continuum theory,[14] the calculation of rates and kinetic isotope effects requires the gas phase valence bond matrix elements and the outer-sphere reorganization energy matrix elements. The gas phase valence bond matrix elements are represented by molecular mechanical terms fit to available experimental data. The outer-sphere reorganization energy matrix elements are calculated with an electrostatic dielectric continuum model.

The calculation of both the gas phase and the solvation input quantities relies on obtaining qualitatively accurate structures for the reacting ruthenium polypyridyl complexes. For this purpose, we performed geometry optimizations at the DFT/B3LYP level[24] with the SBKJC(d) basis set[25] for $[(bpy)_2(py)Ru^{IV}O]^{2+}$, $[(bpy)_2(py)Ru^{II}OH_2]^{2+}$, $[(tpy)(bpy)Ru^{IV}O]^{2+}$, $[(tpy)(bpy)Ru^{II}OH_2]^{2+}$, and $[(tpy)(bpy)Ru^{III}OH]^{2+}$. As is generally accepted, the ruthenium polypyridyl complexes were assumed to be low spin.[26] These calculations were performed using the GAMESS electronic structure package.[27] The resulting Ru−O

(20) Ito, T.; Hamaguchi, T.; Nagino, H.; Yamaguchi, T.; Kido, Hiroaki; Zavarine, I. S.; Richmond, T.; Washington, J.; Kubiak, C. P. *J. Am. Chem. Soc.* **1999**, *121*, 4625.
(21) Rajendran, T.; Thanasekaran, P.; Rajagopal, S.; Gnanaraj, G. A.; Srinivasan, C.; Ramamurthy, P.; Venkatachalapathy, B.; Manimaran, B.; Lu, K.-L. *Phys. Chem. Chem. Phys.* **2001**, *3*, 2063.
(22) Moyer, B. A.; Meyer, T. J. *Inorg. Chem.* **1981**, *20*, 436.
(23) Gilbert, J.; Roecker, L.; Meyer, T. J. *Inorg. Chem.* **1987**, *26*, 1126.
(24) Lee, C.; Yang, W.; Parr, P. G. *Phys. Rev. B* **1988**, *45*, 785. Becke, A. D. *J. Chem. Phys.* **1993**, *98*, 5648. Stephens, P. J.; Devlin, F. J.; Chablowski, C. F.; Frisch, M. J. *J. Phys. Chem.* **1994**, *98*, 11623.
(25) Stevens, W. J.; Krauss, M.; Basch, H.; Jasien, P. G. *Can. J. Chem.* **1992**, *70*, 612.
(26) Huheey, J. E. *Inorganic Chemistry*, 3rd ed.; Harper and Row: New York, 1983.

Table 1. Distances (in Å) for the Models Representing the Three Reactions Defined in Figure 1

	Ru_D-O_D[a]	O_D-O_A[b]	O_A-Ru_A[a]	Ru_D-Ru_A
CompA	2.25	2.70	1.78	6.73
CompB	2.24	2.64	1.78	6.66
Cross	2.25	2.62	1.95	6.82

[a] Distances determined from geometry optimization at the DFT/B3LYP level. [b] Distances determined by fitting to experimentally measured relative rates and kinetic isotope effects.

distances for the three reactions are given in Table 1. These distances may be compared to values from X-ray crystallography studies on related complexes. In particular, this distance has been experimentally measured as 1.805 and 1.815 Å in $[(bpy)(X)Ru^{IV}O]^{2+}$ complexes[28,29] and 2.151 and 2.168 Å, respectively, in $[(tpy)(X)Ru^{II}-OH_2]^{2+}$ and $[(bpy)(X)Ru^{II}-OH_2]^{2+}$ complexes.[30,29] (Here X is a different ligand in each case.) The calculated distances reported in Table 1 reproduce this trend for the two different ligands (water and oxygen). Note that we also performed these calculations at the RHF and ROHF levels with the SBKJC(d) basis set and obtained distances of 1.75, 2.24, and 2.29 Å for the $Ru^{IV}-O$, $Ru^{III}-OH$, and $R^{II}-OH_2$ bonds, respectively.

The gas-phase valence bond matrix elements are based on a five-site model for the hydrogen-bonded ruthenium complexes:

$$Ru_D - O_D - H - O_A - Ru_A$$

where the D and A subscripts denote donor and acceptor, respectively. The distances within this five-site model are given in Table 1. As discussed above, the Ru−O distances are determined from electronic structure calculations on the individual ruthenium polypyridyl complexes. (For consistency with the gas phase parameters given below, the Ru−O distances were symmetrized. We found that this does not affect the overall results.) The O−O distances were not determined with electronic structure calculations since the two positively charged ruthenium complexes repel each other and do not form a hydrogen bond in the gas phase. Thus, the O−O distances were varied to fit the experimentally measured relative rates and kinetic isotope effects for the three reactions. We emphasize that this five-site model is used only to provide molecular mechanical functional forms for the gas phase matrix elements. As will be described below, all atoms of the ruthenium polypyridyl complexes are included for the calculation of solvation properties.

The diagonal matrix elements are expressed as

$$(h_0)_{1a,1a} = U^{\text{Morse}}_{O_DH} + U^{\text{rep}}_{O_AH} + U^{\text{Coul}}_{1a}$$

$$(h_0)_{1b,1b} = U^{\text{Morse}}_{O_AH} + U^{\text{rep}}_{O_DH} + U^{\text{Coul}}_{1b} + \Delta E_{1b}$$

$$(h_0)_{2a,2a} = U^{\text{Morse}}_{O_DH} + U^{\text{rep}}_{O_AH} + U^{\text{Coul}}_{2a} + \Delta E_{2a}$$

$$(h_0)_{2b,2b} = U^{\text{Morse}}_{O_AH} + U^{\text{rep}}_{O_DH} + U^{\text{Coul}}_{2b} + \Delta E_{2b} \qquad (13)$$

(Note that the dependence of the matrix elements on the proton coordinate r_p is suppressed in eq 13 for clarity.) The Morse potential for an O−H bond of length R_{OH} is

$$U^{\text{Morse}}_{OH}(r_p) = D_{OH}(1 - e^{-\beta_{OH}(R_{OH}-R^o_{OH})})^2 \qquad (14)$$

where $D_{OH} = 102.0$ kcal/mol, $\beta_{OH} = 2.35$ Å^{-1}, and $R^o_{OH} = 0.96$ Å. These values were chosen to be consistent with the experimental dissociation energy, frequency, and equilibrium bond length for typical O−H bonds.[31] The repulsion term between nonbonded atoms O and H separated by distance R_{OH} is

$$U^{\text{rep}}_{OH}(r_p) = D'_{OH}e^{-\beta'_{OH}R_{OH}} \qquad (15)$$

where $\beta'_{OH} = 2.5$ Å^{-1} and $D'_{OH} = 500$ kcal/mol. The parameters for both the Morse and repulsion terms are similar to those used by Warshel and co-workers for related types of bonds.[31]

The Coulomb interaction potential between the transferring H atom and the other sites is

$$U^{\text{Coul}}_i(r_p) = \sum_k \frac{q^i_k q_H e^2}{R_{kH}} \qquad (16)$$

where $\sum_k$ is a sum over all sites except the transferring hydrogen and the oxygen bonded to the hydrogen, R_{kH} is the distance between the hydrogen atom and site k, q_H is the charge assigned to the hydrogen, and q^i_k is the charge on site k for diabatic state i. For all diabatic states, the charge on the hydrogen is +0.4. For the comproportionation reactions, the charges on the oxygen sites are −1.4 and −1.0 for the bonding and nonbonding atoms, respectively. For the Cross reaction, the charges on the oxygen sites are −0.4 and −1.0 for the bonding and nonbonding atoms, respectively. The charges on the ruthenium sites were chosen to ensure the correct charge on each complex for the diabatic states.

The constants ΔE_{1b}, ΔE_{2a}, and ΔE_{2b} are fit to reproduce the experimentally determined driving forces (i.e., reaction free energies) for PCET and ET, respectively. For the CompA reaction, the experimentally determined reaction free energies are $\Delta G^o_{PCET} = -2.5$ kcal/mol and $\Delta G^o_{ET} \geq 12.7$ kcal/mol (where we assume the equality for this paper).[7,8] For the CompB reaction, the experimentally determined reaction free energy is $\Delta G^o_{PCET} = -2.51$ kcal/mol,[9] and we assume that $\Delta G^o_{ET} = 12.7$ kcal/mol (as experimentally determined for the CompA reaction). For the Cross reaction, the experimentally determined reaction free energies are $\Delta G^o_{PCET} = -1.3$ kcal/mol and $\Delta G^o_{ET} = 11$ kcal/mol.[8] Within the multistate continuum theory, $\Delta G^o_{ET} = \Delta G^o_{1a\rightarrow 2a}$ and $\Delta G^o_{PCET} = \Delta G^o_{1a\rightarrow 2b}$, where $\Delta G^o_{i\rightarrow j}$ is the free energy difference between the solvated diabatic states j and i at the equilibrium solvent coordinates. These diabatic free energy differences are easily calculated within the multistate continuum theory.[4,14] Our model is parametrized to reproduce the experimentally measured values of ΔG^o_{PCET} and ΔG^o_{ET} for the three reactions. The driving force for PT is not experimentally available and is determined by assuming the free energy difference between PT states is independent of the ET state: $\Delta G^o_{1a\rightarrow 1b} = \Delta G^o_{2b\rightarrow 2a}$. Thus, $\Delta G^o_{PT} = \Delta G^o_{1a\rightarrow 1b} = 15.2$, 15.21, and 12.3 kcal/mol, respectively, for the CompA, CompB, and Cross

(27) Schmidt, M. W.; Baldridge, K. K.; Boatz, J. A.; Elbert, S. T.; Gordon, M. S.; Jensen, J. H.; Koseki, S.; Matsunaga, N.; Nguyen, K. A.; Su, S.; Windus, T. L.; Dupuis, M.; Montgomery, J. A. *J. Comput. Chem.* **1993**, *14*, 1347.
(28) Welch, T. W.; Ciftan, S. A.; White, P. S.; Thorp, H. H. *Inorg. Chem.* **1997**, *36*, 4812.
(29) Cheng, W.-C.; Yu, W.-Y.; Cheung, K.-K.; Che, C.-M. *J. Chem. Soc., Dalton Trans.* **1994**, 57.
(30) Grover, N.; Gupta, N.; Singh, P.; Thorp, H. H. *Inorg. Chem.* **1992**, *31*, 2014.
(31) Warshel, A. *Computer Modeling of Chemical Reactions in Enzymes and Solutions;* John Wiley: New York, 1991.

reactions. This approximation is not rigorously valid but is adequate for these reactions since the 1b and 2a states are much higher in energy than the 1a and 2b states.

In this paper, the couplings are assumed to be of the form

$$(h_o)_{1a,1b} = (h_o)_{2a,2b} = V^{PT}$$

$$(h_o)_{1a,2a} = (h_o)_{1b,2b} = V^{ET} = A_{ET} \exp(-\beta_{ET} R_{RuRu}/2)$$

$$(h_o)_{1a,2b} = (h_o)_{1b,2a} = V^{EPT} \quad (17)$$

The value of the coupling V^{PT} was chosen to be of a magnitude similar to that of the couplings used in other related EVB models and was refined to fit the experimentally measured relative rates and kinetic isotope effects for each reaction. The values for V^{PT} used to obtain the data in this paper were 32.7, 44, and 76 kcal/mol, respectively, for the CompA, CompB, and Cross reactions. (These values are within the range of parameters used in other empirical valence bond treatments of proton transfer reactions.[31]) The trend in the values for the CompA and CompB reactions is consistent with the trend in the O−O distances in that V^{PT} increases as the O−O distance decreases. The value of V^{PT} for the Cross reaction is significantly different from the values for the CompA and CompB reactions because the Cross reaction involves a fundamentally different proton transfer reaction. Specifically, in the Cross reaction, the proton transfers from an OH_2 to an OH ligand, while in the CompA and CompB reactions, the proton transfers from an OH_2 to an O ligand. The value of A_{ET} is not required since we are calculating only relative rates and kinetic isotope effects. The electronic coupling depends on the Ru−Ru distance R_{RuRu}, however, and we estimate the electronic coupling parameter β_{ET} to be 3.0 $Å^{-1}$ based on previous calculations of the electronic coupling for electron transfer in model systems.[32] Within the framework of valence bond theory, V^{EPT} is expected to be significantly smaller than V^{ET} since V^{EPT} is a second-order coupling and V^{ET} is a first-order coupling. For simplicity, in this paper V^{EPT} was approximated as zero. As discussed in ref 17, the overall coupling for a PCET reaction is approximately proportional to V^{ET} when $V^{EPT} = 0$.

The solvent reorganization energies are calculated with the frequency-resolved cavity model (FRCM) developed by Newton, Rostov, and Basilevsky.[33,34] This approach allows for distinct effective solute cavities pertaining to the optical and inertial solvent response. The cavities are formed from spheres centered on all of the atoms. The two effective radii for the solute atoms are defined as $r_\infty = \kappa\, r_{vdW}$ and $r_{in} = r_\infty + \delta$, where r_{vdW} is the van der Waals radius, κ is a universal scaling factor, and δ is a constant specific to the particular solvent. As given in ref 34, $\kappa = 0.9$ and $\delta = 0.9$ for cations in water. The static and optical dielectric constants of water at 298 K are $\epsilon_o = 78.4$ and $\epsilon_\infty = 1.78$.[34] As mentioned above, all atoms of the ruthenium polypyridyl complexes are included for the calculation of the solvation properties. The charge density of each diabatic (i.e., valence bond) state is defined by assigning appropriate partial charges to all atoms. The reorganization energy matrix element between diabatic states i and j is determined by calculating the interaction of the charge density of state i with the dielectric continuum solvent response to the charge density of state j.

The atomic coordinates utilized for the FRCM calculations in this paper were obtained by combining the two reacting ruthenium complexes with structures determined from the electronic structure calculations described above. (The outer-sphere theory of PCET used in this paper requires the solute nuclei other than the transferring hydrogen to be fixed. As mentioned above, the effects of inner-sphere reorganization may easily be included in the rate expression but are neglected in this paper for simplicity.) The two reacting ruthenium complexes were combined manually by placing the Ru−O−H−O−Ru on a line and rotating the complexes to maximize the symmetry reflected through the hydrogen-bonding interface. We found that altering the orientation between the two complexes and shifting the internal coordinates within the complexes to represent different ruthenium oxidation states does not significantly impact the outer-sphere reorganization energies. The O−O distances between the reacting ruthenium complexes were determined by fitting to the experimentally measured relative rates and kinetic isotope effects.

The atomic charges for the diabatic states used for the FRCM calculations in this paper were designated as follows. The ruthenium atom was assigned a charge of +2, +3, or +4 corresponding to the appropriate oxidation state. The atomic charges on the pyridyl ligands were obtained by performing electronic structure calculations on the isolated ligands at the DFT/B3LYP/6-31G**[35] level. The geometries of the isolated ligands were optimized by imposing C_{2v} symmetry, and the atomic charges were calculated with the CHELPG method[36] for the optimized ligands. (These calculations were performed with Gaussian98.[37]) The partial charges for the oxygen-containing ligands were chosen such that all hydrogen atoms were assigned a charge of +0.4 and the oxygen atoms were assigned charges resulting in an overall charge of −2, −1, and 0, respectively, for the O, OH, and OH_2 ligands. Note that this assignment neglects charge transfer between the ruthenium and the ligands. Although this charge transfer is substantial, this simplification to the charge distribution does not qualitatively alter the calculated outer-sphere reorganization energies.[17]

The rate constant for a bimolecular (second-order) reaction may be expressed as[38,39]

$$k_{bi} = K_A(r) k_{uni} \quad (18)$$

where $K_A(r)$ is the equilibrium constant for the formation of

(32) Henderson, T. M.; Cave, R. J. *J. Chem. Phys.* **1998**, *109*, 7414.
(33) Basilevsky, M. V.; Rostov, I. V.; Newton, M. D. *Chem. Phys.* **1998**, *232*, 189−199.
(34) Newton, M. D.; Basilevsky, M. V.; Rostov, I. V. *Chem. Phys.* **1998**, *232*, 201−210.
(35) Ditchfield, R.; Hehre, W. J.; Pople, J. A. *J. Chem. Phys.* **1971**, *54*, 724. Hehre, W. J.; Ditchfield, R.; Pople, J. A. *J. Chem. Phys.* **1972**, *56*, 2257. Francl, M. M.; Petro, W. J.; Hehre, W. J.; Binkley, J. S.; Gordon, M. S.; DeFrees, D. J.; Pople, J. A. *J. Chem. Phys.* **1982**, *77*, 3654.
(36) Breneman, C. M.; Wiberg, K. B. *J. Comput. Chem.* **1990**, *11*, 361.
(37) Frisch, M. J.; Trucks, G. W.; Schlegel, H. B.; Scuseria, G. E.; Robb, M. A.; Cheeseman, J. R.; Zakrzewski, V. G.; Montgomery, J. A., Jr.; Stratmann, R. E.; Burant, J. C.; Dapprich, S.; Millam, J. M.; Daniels, A. D.; Kudin, K. N.; Strain, M. C.; Farkas, O.; Tomasi, J.; Barone, V.; Cossi, M.; Cammi, R.; Mennucci, B.; Pomelli, C.; Adamo, C.; Clifford, S.; Ochterski, J.; Petersson, G. A.; Ayala, P. Y.; Cui, Q.; Morokuma, K.; Malick, D. K.; Rabuck, A. D.; Raghavachari, K.; Foresman, J. B.; Cioslowski, J.; Ortiz, J. V.; Stefanov, B. B.; Liu, G.; Liashenko, A.; Piskorz, P.; Komaromi, I.; Gomperts, R.; Martin, R. L.; Fox, D. J.; Keith, T.; Al-Laham, M. A.; Peng, C. Y.; Nanayakkara, A.; Gonzalez, C.; Challacombe, M.; Gill, P. M. W.; Johnson, B. G.; Chen, W.; Wong, M. W.; Andres, J. L.; Head-Gordon, M.; Replogle, E. S.; Pople, J. A. *Gaussian 98*, revision A.6; Gaussian, Inc.: Pittsburgh, PA, 1998.
(38) Newton, M. D.; Sutin, N. *Annu. Rev. Phys. Chem.* **1984**, *35*, 437.
(39) Sutin, N. *Prog. Inorg. Chem.* **1983**, *30*, 441.

the precursor complex (with separation distance r) and k_{uni} is the unimolecular (first-order) rate constant within this complex. (Note that this expression is valid only if the dissociation of the precursor complex is much faster than the unimolecular reaction.) A more accurate form of this expression would include the integration over all separation distances r, rather than assuming a single optimal effective separation distance. The equilibrium constant $K_A(r)$ may be expressed in terms of the work required to bring two charged spheres together in a dielectric continuum solvent. Although the value of $K_A(r)$ for a given r is expected to be the same for hydrogen and deuterium, the optimal effective separation distance r in eq 18 may vary for hydrogen and deuterium due to differences in k_{uni}. In addition, the value of $K_A(r)$ will impact the relative rates due to differences in the optimal effective separation distance r for the three reactions. We have found that the effect of this factor on the kinetic isotope effects and relative rates is negligible. Moreover, the experimental relative rates were obtained by correcting for different ionic strengths under the assumption of the same average effective diameter of the ions for all three reactions.[40,41] Thus, for consistency we do not include effects of $K_A(r)$ in this paper. In addition, we point out that this approach neglects the different energetics of formation of the hydrogen-bonded complexes for the three reactions. These differences are not expected to significantly impact the kinetic isotope effects but could impact the relative rates of the three reactions as a result of varying proton donor−acceptor distances.

In this paper, our goal is to develop an empirical, self-consistent model for the CompA, CompB, and Cross reactions. For this purpose, five parameters were fit to reproduce five independent experimentally measured quantities. First the O−O distance for the CompA reaction was set to 2.7 Å and V^{PT} was varied to reproduce the experimental kinetic isotope effect. Second, the O−O distance and V^{PT} for the CompB reaction were varied to fit the experimental kinetic isotope effect and rate relative to the CompA reaction. Third, the O−O distance and V^{PT} for the Cross reaction were varied to fit the experimental kinetic isotope effect and rate relative to the CompA reaction. Note that the O−O distances and couplings V^{PT} were restricted to physically reasonable, self-consistent values. Moreover, the O−O distances and couplings V^{PT} influence the rates and kinetic isotope effects in a complex manner, and we found that only a limited range of parameter values adequately reproduces the experimental data.

III. Results and Discussion

A comparison between the theoretical calculations and the experimental data for the three reactions is given in Table 2. This table indicates that the theory accurately reproduces the kinetic isotope effects and relative rates for all three reactions. As discussed above, this agreement is due to the fitting of the O−O distances and the couplings V^{PT} to reproduce the experimentally measured kinetic isotope effects and relative rates. The values of the O−O distances required to reproduce the experimental data provide insight into the physical basis for the kinetic isotope effects and relative rates.

Table 1 indicates that the O−O distance used in our model to reproduce the experimental data is largest for the CompA reaction and shortest for the Cross reaction. (Note that the quantitative values of the O−O distances depend on the details of the model system, so only the trend is meaningful.) As illustrated in Figure 2, this prediction is consistent with the degree of steric crowding near the oxygen proton acceptor for the three reactions.[9] The CompA reaction involves the $[(bpy)_2(py)Ru^{IV}O]^{2+}$ complex, which has substantial steric crowding near the oxygen due to the (bpy) and (py) ligands. In contrast, the CompB reaction involves the $[(tpy)(bpy)Ru^{IV}O]^{2+}$ complex, which has much less steric crowding near the oxygen due to the (tpy) ligand that replaces the (bpy)(py) ligands. Finally, the

Table 2. Comparison between Theory and Experiment for the Kinetic Isotope Effects and Relative Rates for the Three Reactions Defined in Figure 1

	KIE		relative rate[a]	
	theory	experiment	theory	experiment[b]
CompA	16.0	16.1 ± 0.4[c]	1.0	1.0[c]
CompB	11.3	11.4 ± 1.3[d]	9.8	9.6[d]
Cross	6.1	5.8 ± 0.4[d]	6.2	6.1[c]

[a] The rates are calculated relative to the CompA reaction. [b] The experimental relative rates are corrected for differences in ionic strengths using the relation given in ref 40. The average effective diameter is determined from experimental data for the CompA reaction at two different ionic strengths[8] and is approximated to be the same for all three reactions.[41] [c] Experimental value obtained from ref 8. [d] Experimental value obtained from ref 9.

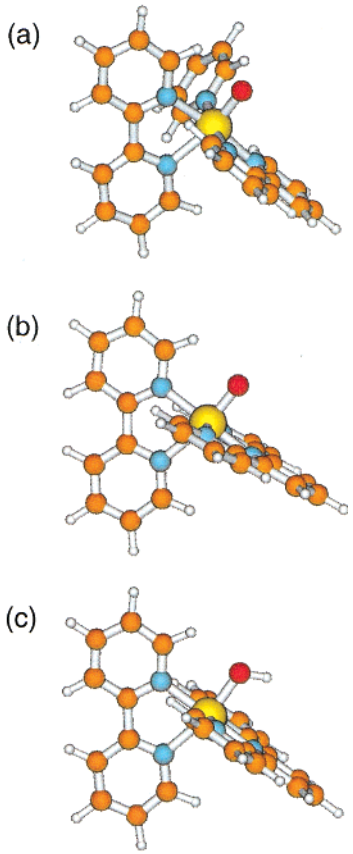

Figure 2. Structures optimized at the DFT/B3LYP level for (a) $[(bpy)_2(py)Ru^{IV}O]^{2+}$, (b) $[(tpy)(bpy)Ru^{IV}O]^{2+}$, and (c) $[tpy)(bpy)Ru^{III}OH]^{2+}$. The structure in (a) has more steric crowding near the oxygen than that in (b) due to the different ligands. The structure in (b) has more steric crowding near the oxygen than that in (c) since the Ru═O distance is shorter than the Ru−OH distance. As a result, when each of these complexes hydrogen bonds to the OH_2 of another ruthenium polypyridyl complex, the O−O distance is longest for (a) and shortest for (c).

(40) Jordan, R. B. *Reaction Mechanisms of Inorganic and Organometallic Systems;* Oxford University Press: New York, 1991; p 19.
(41) Farrer, B. T.; Thorp, H. H., private communication.

Cross reaction involves the $[(tpy)(bpy)Ru^{III}OH]^{2+}$ complex, which has even less steric crowding near the oxygen due to the significantly longer Ru−O distance for the OH ligand (1.95 Å) than for the O ligand (1.78 Å). For the reactions shown in Figure 1, each of these ruthenium complexes hydrogen bonds to another ruthenium complex with a water ligand. The O−O distance in this hydrogen bond increases as the steric crowding near the oxygen proton acceptor increases. Thus, these steric effects provide a physical basis for the trend in the O−O distances for our model systems.

Figure 3 depicts slices of the two-dimensional free energy surfaces as functions of the collective solvent coordinates with hydrogen and deuterium for the three reactions. On the right side of each set of free energy surfaces is the product hydrogen (or deuterium) potential energy curve and the corresponding vibrational wave functions. (The contributions of the various product states to the overall rate are given in Table 3.) This figure shows that the splittings between the vibrational states are smaller for deuterium than for hydrogen, leading to qualitatively different excited vibrational wave functions. This figure also indicates that the product hydrogen potential energy curve becomes less asymmetric as the O−O distance decreases, leading to greater delocalization of the vibrational wave functions.

Figure 4 depicts the reactant and product vibrational wave functions for the lowest energy states for the three reactions. This figure illustrates that the overlap between these vibrational wave functions increases as the O−O distance decreases. Specifically, this figure indicates that the overlap is smallest for the CompA reaction (which has the largest O−O distance) and largest for the Cross reaction (which has the smallest O−O distance). This figure also shows that the overlap is smaller for deuterium than for hydrogen. The quantitative values for the overlap integrals are given in Table 3.

The relative rates and kinetic isotope effects for these reactions may be analyzed in terms of the rate expression given in eq 7. For each pair of states, the rate is proportional to the product of the exponential of the free energy barrier ($e^{-\Delta G^{\dagger}_{\mu\nu}/kT}$) and the square of the overall coupling ($V^2_{\mu\nu}$). As given in eq 8, the free energy barrier depends on the reaction free energy $\Delta G^{o}_{\mu\nu}$ and the outer-sphere reorganization energy $\lambda_{\mu\nu}$. As given in eq 12, the coupling may be approximated by the product of the electronic coupling ($V^{ET} = A_{ET}e^{-\beta_{ET}R_{RuRu}/2}$) and the overlap of the reactant and product vibrational wave functions ($\langle\phi^{I}_{\mu}|\phi^{II}_{\nu}\rangle_p$). Table 3 gives these various terms for the lowest energy reactant and product states (i.e., $\mu = \nu = 1$). The terms for the higher product states are given in the Supporting Information.

As shown in Table 2, the CompA reaction is slower than the CompB reaction. The physical basis for this relation is provided in Table 3. The reaction free energy ΔG^{o}_{11} is the same for the CompA and CompB reactions. The outer-sphere reorganization energy λ_{11} is slightly larger for the CompB reaction than for the CompA reaction due to greater solvent accessibility for the CompB reacting complex, as illustrated in Figure 2. This difference leads to a slightly larger free energy barrier for the CompB reaction and thus decreases the rate for the CompB relative to the CompA reaction (as seen by a comparison of $e^{-\Delta G^{\dagger}_{11}/kT}$). The electronic coupling V^{ET} is slightly larger for the CompB than for the CompA reaction due to the slightly shorter Ru−Ru distance for the CompB reaction (as seen by a comparison of $e^{-\beta_{ET}R_{RuRu}}$). On the other hand, the shorter O−O distance for the CompB reaction leads to a substantially larger overall coupling $V_{\mu\nu}$ due to the larger overlap of the reactant

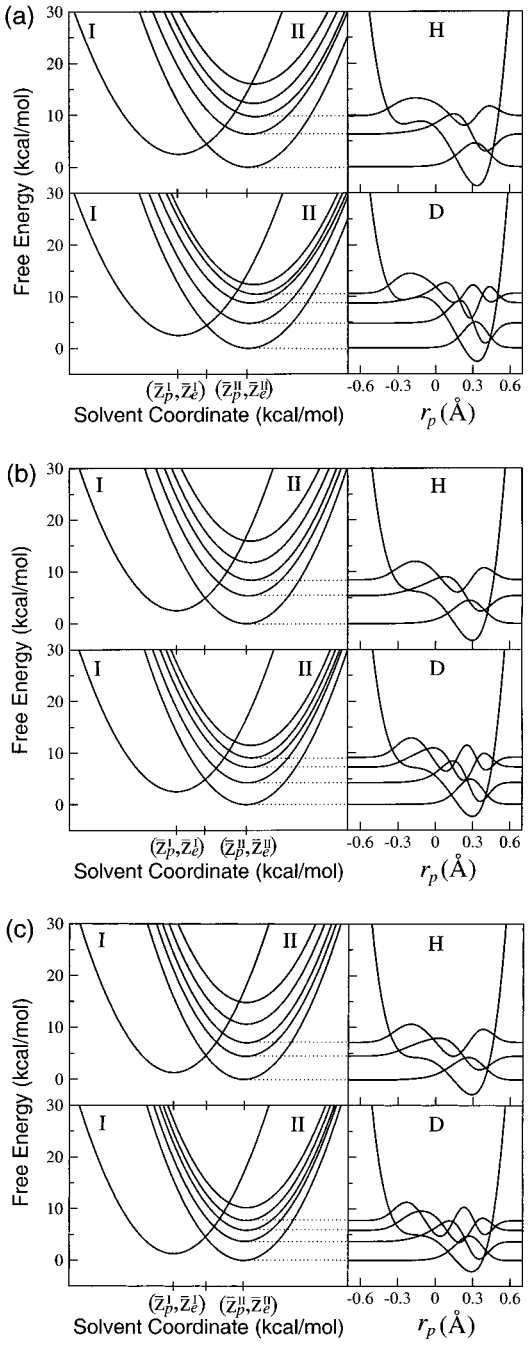

Figure 3. Slices of the two-dimensional ET diabatic free energy surfaces for the (a) CompA, (b) CompB, and (c) Cross reactions. The top frame of each figure was calculated with hydrogen, while the bottom frame of each figure was calculated with deuterium. The slices were obtained along the line connecting the minima of the lowest energy reactant (I) and product (II) two-dimensional free energy surfaces. On the left of each figure are the free energy surfaces as functions of the solvent coordinates, including the lowest energy reactant (1) free energy surface and the lowest five product (II) free energy surfaces. On the right are the product (II) proton potential energy curves and the corresponding proton vibrational wave functions as functions of the proton coordinate r_p evaluated at the minimum of the ground state product free energy surface. Note that the energies associated with the proton vibrational wave functions coincide with the energies of the product free energy surfaces.

Table 3. Analysis of the Theoretical Calculations for the Three Reactions Studied

	isotope	% product states 1/2/3/4[a]	ΔG^{o}_{11} [b]	λ_{11} [c]	$e^{-\Delta G^{\dagger}_{11}/kT}$ [d]	$\lvert\langle\phi_1^{I}\rvert\phi_1^{II}\rangle\rvert^2$ [e]	$e^{-\beta_{ET}R_{RuRu}}$ [f]
CompA	H	73/18/9/0	−2.5	12.37	3.60×10^{-2}	8.69×10^{-5}	1.70×10^{-9}
	D	6/10/18/62	−2.5	12.27	3.75×10^{-2}	4.08×10^{-7}	1.70×10^{-9}
CompB	H	75/21/4/0	−2.5	14.24	1.69×10^{-2}	1.59×10^{-3}	2.10×10^{-9}
	D	17/27/37/19	−2.5	14.09	1.80×10^{-2}	2.99×10^{-5}	2.10×10^{-9}
Cross	H	70/26/4/0	−1.3	15.76	3.84×10^{-3}	6.80×10^{-3}	1.30×10^{-9}
	D	15/30/46/9	−1.3	15.52	4.09×10^{-3}	2.27×10^{-4}	1.30×10^{-9}

[a] This refers to the percentage contribution of the lowest four product states to the overall rate, where the lowest energy product state is indicated by 1. These numbers do not always add up to 100% due to contributions from higher states. [b] The equilibrium free energy difference $\Delta G^{o}_{\mu\nu}$ is defined in eq 9.[c] The outer-sphere reorganization energy $V_{\mu\nu}$ is defined in eq 10. [d] The free energy barrier $\Delta G^{\dagger}_{\mu\nu}$ is defined in eq 8. [e] This vibrational overlap factor contributes to the overall coupling $V_{\mu\nu}$ defined in eq 11 and approximated in eq 12. [f] The factor $e^{-\beta_{ET}R_{RuRu}}$ is the distance-dependent part of the square of the electronic coupling V^{ET}, which contributes to the overall coupling $V_{\mu\nu}$.

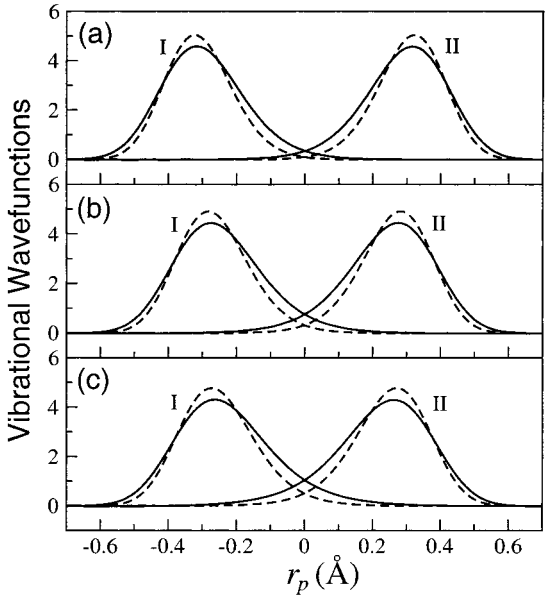

Figure 4. Reactant (I) and product (II) vibrational wave functions for H (solid) and D (dashed) for the (a) CompA, (b) CompB, and (c) Cross reactions. For each reaction, the overlap is larger for H than D. The overlap for a given isotope is smallest for (a) and largest for (c) since the O−O distance is largest for the reaction in (a) and smallest for that in (c).

and product vibrational wave functions (as seen by a comparison of the square of this overlap $|\langle\phi_1^{I}|\phi_1^{II}\rangle_p|^2$). This difference in coupling dominates the relative rates for the CompA and CompB reactions. As a result, the CompB reaction is nearly one order of magnitude faster than the CompA reaction.

In addition, as shown in Table 2, the rate of the Cross reaction is greater than the CompA reaction but less than the CompB reaction. The Ru−Ru distance is larger for the Cross reaction (6.82 Å) than for the CompA and CompB reactions (6.73 and 6.66 Å, respectively). This difference in Ru−Ru distances is due to the larger Ru−O distance for the OH ligand than for the O ligand. The free energy barrier $\Delta G^{\dagger}_{11}$ is substantially higher for the Cross reaction since the driving force is less exoergic (as determined experimentally) and the outer-sphere reorganization energy is larger (due to the larger Ru−Ru distance). This higher free energy barrier is evident in Figure 3. Although the electronic coupling V^{ET} is smaller for the Cross reaction due to the larger Ru−Ru distance, the shorter O−O distance for the Cross reaction leads to a larger overlap of the reactant and product vibrational wave functions, resulting in a substantially larger overall coupling $V_{\mu\nu}$. The higher free energy barrier slows down the rate, while the larger coupling speeds up the rate for the Cross reaction relative to the CompA and CompB reactions. As a result of the balance between these competing effects, the Cross reaction is faster than the CompA reaction but slower than the CompB reaction.

Previous theoretical calculations predicted that the kinetic isotope effect for PCET reactions will increase as the proton donor−acceptor distance increases.[16,42] The basis for this prediction is that the rate for each pair of states is approximately proportional to the square of the overlap between the reactant and product vibrational wave functions. (This may be seen by substituting eq 12 into eq 7.) Thus, the kinetic isotope effect for each pair of states is approximately proportional to the square of the ratio of the overlap for hydrogen to the overlap for deuterium. This ratio becomes larger as the overlap becomes smaller (i.e., as the proton donor−acceptor distance increases). The overall kinetic isotope effect is not simply proportional to this ratio, however, due to contributions from several product states to the overall rate. The relative contributions from the various product states are determined by a competition between the coupling $V_{\mu\nu}$, which favors higher energy product states with larger overlap between the reactant and product vibrational wave functions, and the free energy barrier $\Delta G^{\dagger}_{\mu\nu}$, which favors lower energy product states. Since the overlap between reactant and product vibrational wave functions for the lowest energy product state is smaller for deuterium than for hydrogen, typically the contribution of the lowest energy product state is smaller for deuterium than for hydrogen.

As shown in Table 2, the kinetic isotope effect is largest for the CompA reaction and smallest for the Cross reaction. This trend is due to the differences in the O−O distances. As illustrated by Figure 4, the overlap is smallest for the CompA reaction (with the largest O−O distance) and largest for the Cross reaction (with the smallest O−O distance). Moreover, both Figure 4 and Table 3 indicate that the ratio of the overlap for hydrogen to the overlap for deuterium is largest for the CompA reaction and smallest for the Cross reaction. As discussed above, however, the overall kinetic isotope effect is not proportional to this ratio due to the contributions of the other product states to the overall rate. Table 3 shows that for hydrogen the lowest product state contributes 70−75% to the overall rate for all three reactions. In contrast, for deuterium, the contribution of the lowest product state to the overall rate is significantly smaller. This phenomenon is due to the smaller overlap between the reactant and product vibrational wave functions for deuterium (as illustrated in Figure 4) and the

(42) Note that this prediction applies only to the regime in which the proton transfers.

smaller splittings between the vibrational states for deuterium (as illustrated in Figure 3). Note that the kinetic isotope effect would be significantly larger if the lowest product state dominated for both hydrogen and deuterium.

IV. Conclusions

In this paper, an empirical self-consistent model was developed for three PCET reactions in ruthenium polypyridyl complexes (denoted the CompA, CompB, and Cross reactions). Based on the values of the proton donor−acceptor distances required to reproduce the experimental data, the model predicts that the proton donor−acceptor distance (i.e., the O−O distance) is largest for the CompA reaction and smallest for the Cross reaction. This prediction is consistent with the degree of steric crowding near the oxygen proton acceptor for the three reactions. An analysis of the calculations illustrates the differences among the three reactions in terms of the solvent reorganization energy, the free energy barrier, the coupling between the electron transfer states, the overlap between the reactant and product vibrational wave functions, and the relative contributions of the product states. This analysis elucidates the underlying physical basis for the experimentally observed trends in the rates and kinetic isotope effects, as well as for the unusually high magnitude of the kinetic isotope effects.

These theoretical calculations provide insight into the experimental observation that the CompB reaction is nearly one order of magnitude faster than the CompA reaction, and the Cross reaction is in the intermediate regime. The analysis implies that the dominant factor contributing to the faster rate of the CompB reaction relative to the CompA reaction is the larger overlap between the reactant and product proton vibrational wave functions for the CompB reaction. In this model, the overlap is larger for the CompB reaction since the O−O distance is smaller for the CompB reaction than for the CompA reaction. (Note that all other aspects of these reactions are very similar.) According to this theoretical formulation, a larger overlap between the reactant and product proton vibrational wave functions leads to a larger overall coupling between the lowest energy reactant and product states and hence increases the rate. The analysis implies that the rate of the Cross reaction is in the intermediate regime due to a balance between competing factors: the shorter O−O distance increases the rate, while the smaller driving force and larger Ru−Ru distance decrease the rate. (Note that the trends for the Cross reaction are less certain since the Cross reaction is fundamentally different from the CompA and CompB reactions.)

Furthermore, these theoretical calculations provide insight into the experimental observation that the kinetic isotope effect is largest for the CompA reaction and smallest for the Cross reaction. The analysis implies that the dominant factor contributing to this trend is the overlap between the reactant and product proton vibrational wave functions. According to this theoretical formulation, the kinetic isotope effect for each pair of states is approximately proportional to the square of the ratio of hydrogen to deuterium vibrational wave function overlap. In general, this overlap ratio increases as the overlap between the reactant and product hydrogen vibrational wave functions decreases (i.e., as the proton donor−acceptor distance increases when all other aspects are similar).[42] In this model, the overlap ratio is largest for the CompA reaction and smallest for the Cross reaction since the O−O distance is largest for the CompA reaction and smallest for the Cross reaction.

These calculations also provide an explanation for the unsually large magnitude of the kinetic isotope effects for oxoruthenium polypyridyl complexes. Although the proton donor−acceptor distance strongly influences the magnitude of the kinetic isotope effect, a variety of other factors are also important.[16] For example, despite similar proton donor−acceptor distances, the experimentally measured kinetic isotope effect for PCET is 2.3 for iron biimidazoline complexes[13] but is up to 16 for the ruthenium polypyridyl complexes studied in this paper. A fundamental difference between the iron biimidazoline systems and the ruthenium polypyridyl systems is the electron donor−acceptor distance. The Fe−Fe distance is 10−11 Å for the iron bi-imidazoline systems, while the Ru−Ru distance is 6−7 Å for the ruthenium polypyridyl systems. The close proximity of the proton transfer interface to the electron donor and acceptor in oxoruthenium complexes results in stronger electrostatic interactions that lead to smaller overlap between the reactant and product proton vibrational wavefunctions. Another factor influencing the kinetic isotope effect is the reaction free energy, which impacts the relative contributions of the product states for hydrogen and deuterium. In general, the kinetic isotope effects for PCET reactions are determined by a combination of these various factors.

Acknowledgment. We thank Dr. Hélène Decornez and Dr. Simon Webb for helpful discussions and assistance with the calculations. We also thank Dr. H. Holden Thorp and Dr. Brian Farrer for assistance with the interpretation of the experiments. We are grateful for financial support from NSF Grant CHE-0096357 and NIH Grant GM56207. S.H.-S. is the recipient of an Alfred P. Sloan Foundation Research Fellowship and a Camille Dreyfus Teacher−Scholar Award.

Supporting Information Available: The analysis of the lowest four product states for the three reactions studied. This material is available free of charge via the Internet at http://pubs.acs.org. See any current masthead page for ordering information and Web access instructions.

JA017633D